Dynamic Autoregressive Neuromagnetic Causality Imaging (DANCI)

Richard E. Frye, M.D., Ph.D.
Departments of Pediatrics and Neurology
University of Texas Health Science Center at Houston
UCT 2478 – 7000 Fannin, Houston, TX 77098
USA

http://www.nmr.mgh.harvard.edu/~richfrye

Meng Hung (Roger) Wu and George Zouridakis, Ph.D.
Biomedical Imaging Laboratory
Department of Computer Science
University of Houston
501 Philip G. Hoffman Hall, Houston TX 77204
USA

http://www2.cs.uh.edu/~zouridakis/

Abstract: - This presentation provides a demonstration of how Granger causality (GC) can be applied to MEG data to visualize dynamic functional connectivity and causality between cortical regions on a millisecond time scale. GC is derived from autoregressive models and provides directionality information. We apply the GC technique to dynamic statistical parameter map source space to demonstrate that the dynamics of neural networks can visualized during a perceptual task. The results from this demonstration coincide with models of speech perception and suggest that Dynamic Autoregressive Neuromagnetic Causality Imaging (DANCI) can be used to investigate and verify theoretical neural network models of brain function.

Key-Words: - Magnetoencephalography; Neural connectivity; Autoregressive modeling; Granger causality; Large-scale neural networks; Neural network dynamics; Cognitive neuroscience; Neuroimaging.

1 Introduction

Developments in advanced neuroimaging techniques have expanded our knowledge of brain function. Over the past two decades, neuroimaging research has concentrates on the location of neural activity, change in gray or white matter volume, metabolic change or lesion. Although this information about neural specialization has been helpful, it has its limitations. The fact that the brain is a large-scale distributed interconnected network points to the fact that the emergent behaviors resulting from cognition processes are probably not located in one part of the brain. Thus, identifying interactions between different areas of the brain is at least, if not more, important than knowing the areas of the brain at which the specific functions occur.

Recently, tools and techniques have become available for studying the integration of large-scale neural systems through visualization of anatomic and functional neural connectivity [1]. Most of these techniques are based on magnetic resonance imaging (MRI) technology. For example, diffusion tensor imaging along with tractography has provided detailed information regarding the organization, integrity and architecture of white matter connectivity in the brain [2]. Although anatomic methods are important for understanding general brain organization and changes in connectivity due to maturation or understanding abnormal brain function in acquired or developmental disorder states, understanding the organization of large-scale neural systems during cognitive processing requires a measure of functional connectivity. Thus, connectivity methods have been applied to neuroimaging techniques that measure changes in brain metabolism due to neural activity, such as functional MRI. Such methods have provided insight into brain function. Indeed, neural systems have been identified with connectivity analyses that were not obvious on functional activation maps [3]. Although connectivity analysis with function MRI data has assisted in the identification of cognitive neural systems, functional MRI measures brain activation on a time scale of seconds while brain systems operate on a millisecond time scale. Thus, quick dynamic

changes in neural connectivity probably cannot be measured using neuroimaging techniques that rely on metabolic change.

Signal processing methods for measuring coherence have been adapted to neuroimaging modalities that measure changes in the electric potential or magnetic field of the brain, such as electroencephalography (EEG) and magnetoencephalography (MEG), respectively. One of the advantages of using techniques with excellent time resolution is the ability to examine the dynamics of causal influences. However, few methods have examined directionality or causality. In addition, most techniques have been applied to sensor space, thereby limiting the ability to localize the activity being studied. This presentation will provide a demonstration of how Granger causality can be applied to MEG data to visualize dynamic functional connectivity and causality between cortical regions on a millisecond time scale.

2. An Approach to Imaging Causality

Granger causality (GC), a measure derived from autoregressive models (ARMs), can provide directionality information. GC has been applied to EEG data but the use of this measure in MEG connectivity analysis has received little attention [4].

2.1 Autoregressive Modeling Assumptions

ARM requires the adherence to several assumptions. First, the assumption of stationarity must be addressed. We use the short-window approach introduced by Ding by removing the time-varying average and normalizing using the standard deviation [5]. Following pre-processing, normality is verified using probability plots. In addition, the third and fourth moment of the distribution are verified to be minimal.

2.2 Model Formulation

Connectivity between selected cortical regions is calculated using ARMs and GC applied to dynamic statistical parameter map (dSPM) data. Each dSPM source is considered a separate time series. This time series is modeled by a separate ARM that represent the sources for each observation (i.e., trial) *o* at each time *t* by previous values of its own activity and the activity of the other sources. For example, the temporal dynamics of the activity of a set of sources *S* can be explained by the ARMs given in Equation (1)

In this model, *P* is the number of lags included in the model (i.e., the model order), which must be less than the number of time points *T*. *S* is the number of sources modeled. An estimate of the model produces the coefficients $A_{1...S,1..S,1...P}$ and the error terms $E_{1...S}$.

$$\begin{aligned}
X_1(t,o) &= \sum_{j=1}^{p} A_{1,1,j} \bullet X_1(t-j,o) + \sum_{j=1}^{p} A_{1,2,j} \bullet X_2(t-j,o) + \ldots + \sum_{j=1}^{p} A_{1,S,j} \bullet X_S(t-j,o) + E_1(t,o) \\
X_2(t,o) &= \sum_{j=1}^{p} A_{2,1,j} \bullet X_1(t-j,o) + \sum_{j=1}^{p} A_{2,2,j} \bullet X_2(t-j,o) + \ldots + \sum_{j=1}^{p} A_{2,S,j} \bullet X_S(t-j,o) + E_2(t,o) \\
&\ldots\ldots \\
X_S(t,o) &= \sum_{j=1}^{p} A_{S,1,j} \bullet X_1(t-j,o) + \sum_{j=1}^{p} A_{S,2,j} \bullet X_2(t-j,o) + \ldots + \sum_{j=1}^{p} A_{S,S,j} \bullet X_S(t-j,o) + E_S(t,o)
\end{aligned} \quad (1)$$

2.3 Stationarity and Normality

Several assumptions must be made when using ARMs. Most importantly, the mean and variance must be constant over the analysis window. These assumptions are supported by using a short window and subtracting the ensemble mean activation at each time *t* across observations *o*. The stationary assumption is tested for each ARM by examining the unit roots of the time series using the Dickey-Fuller test.

2.4 Model Order

The order of the model and window size was determined by examining the Akaike information criterion (AIC; Equation 2) and the Bayesian information criterion (BIC; Equation 3).

$$AIC = -2 \bullet \log[\det(\Sigma)] + 2S^2P / N \quad (2)$$

$$BIC = -2 \bullet \log[\det(\Sigma)] + log(N)S^2P / N \quad (3)$$

2.5 Granger Causality

The model is designed to simultaneously account for the influence of all considered sources *S* on each other source *S* as well as the influence of each source on itself. For example, for source 1, coefficients $A_{1,1,1...P}$ quantitatively describe the influence of the activity of source 1 on itself, where as the coefficients $A_{1,2,1...P}$ quantitatively describe the influence of the activity of source 2 on source 1, and the coefficient $A_{1,S,1..P}$ quantitatively describe the influence of source S on source 1, etc. Likewise the coefficient $A_{s,1,1...P}$ for source *s* will describe the quantitative influence of source 1 on source *s*.

Since the ARMs presented in (1) allow the influence of all sources to be considered simultaneously, the influence of a source on another that is occurring through correlation with a third source will be considered in the model and the false correlational influence of the sources will be

revealed by the model. As Seth points out, the statistical significance of the quantitative influence of one source on another can be considered [6]. Linear modeling easily allows the consideration of the significance of a set of coefficients *A* by examining the change in the model error *E* when the coefficients of interest are removed from the model. This significance can be measured by calculating the value (4) which is F distributed with *P* and (*O*T* – *S*P* – 1) degrees of freedom. If the coefficients from one source significantly influence another source, then the GC from the first source to the second source will be significant.

$$F_{P,O\bullet T-S\bullet P-1}=\frac{\frac{\sum_{o=1}^{O}\sum_{t=1}^{T}(X_s^R(t,o)-\hat{X}_s^R(t,o))^2-\sum_{o=1}^{O}\sum_{t=1}^{T}(X_s^F(t,o)-\hat{X}_s^F(t,o))^2}{P}}{\frac{\sum_{o=1}^{O}\sum_{t=1}^{T}(X_s^F(t,o)-\hat{X}_s^F(t,o))^2}{O\bullet T-S\bullet P-1}} \quad (4)$$

3. Applications to MEG Imaging

We apply the GC technique to dSPM values that represent brain activation recorded from a whole-head MEG system during a syllable discrimination task. The data analyzed represents the dynamic connectivity that occurs during perception of the first of two syllables. We chose to investigate the connectivity between two regions of the brain, Heschl's gyrus (HG) and the planum temporale (PT) since these areas are known to be important in the perception of language stimuli. Cortical activity in each region was determined by the sources located in these regions as determined by dSPM. dSPM estimates the noise-normalized activity at approximately 3000 sources in each hemisphere every 1.6ms using a ℓ2 minimum norm technique [7]. Fig 1 shows the two cortical regions of interest highlighted in green and the active cortical sources, in and around these regions, colored in red and yellow.

The data were filtered into alpha, beta and gamma frequency bands. Several sets of ARMs were calculated with different model orders and window sizes for each frequency band. The AIC and BIC values were calculated for each of these sets of ARMs. The AIC and BIC values for the gamma range frequency band is shown in Figs 2 and 3. With consideration of these values we chose a window size of 33ms and a model order of 10 for the gamma frequency band. This was due to the fact that the decent of the AIC value became minimal at this combination of values while the BIC value was near its absolute minimum. The window size and model order for other frequency bands were similarly analyzed and considered.

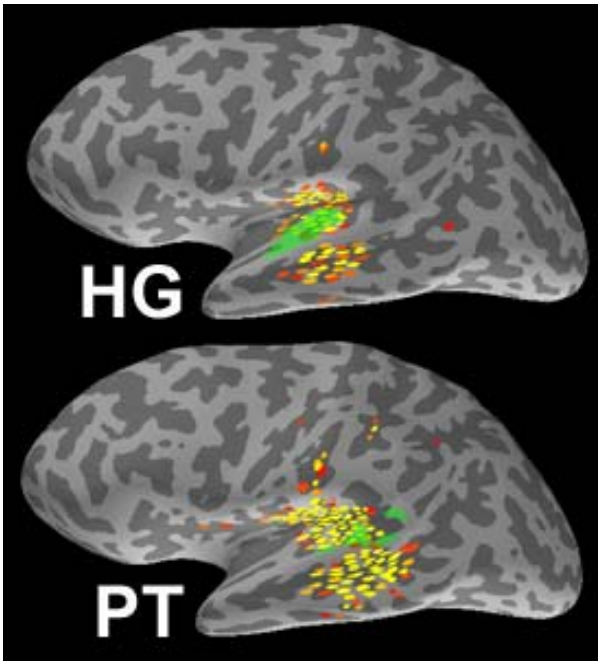

Fig 1. Regions of interest are depicted in green on the inflated cortex with depiction of Heschl's gyrus (HG) above planum temporale (PT). Active dSPM sources are also shown on the inflated cortical surface as yellow and red ovals.

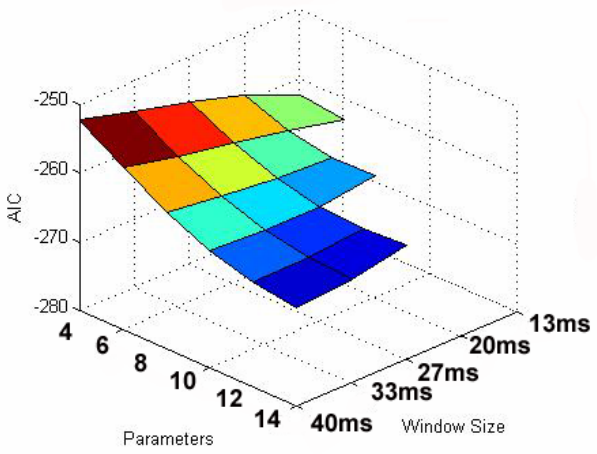

Fig 2. AIC values across model orders and window sizes for the gamma band frequency. Notice that the decent of the AIC slows down considerably with a window size of 33ms and a model order of 10.

Connectivity was visualized in a standardized manner for each time increment *t*. This visualization approach (See Figs 4-8) displays a matrixes of the GC values, as calculated by Equation (4), separately by direction (i.e., HG to PT and HG to PT) in the upper left corner and the causal flows (Sum of In – Sum of Out), which represents the balance of flow though a source, in the upper right

corner. The bottom of the figure depicts connectivity from specific sources in HG to PT and then PT back to HG. Only the connections that are significant at least at the $p < 0.01$ level are displayed, but specific F-values are chosen to optimize the display of significant connections. The color of each line is proportional the F-value as represented in the color bar next to the connection matrixes.

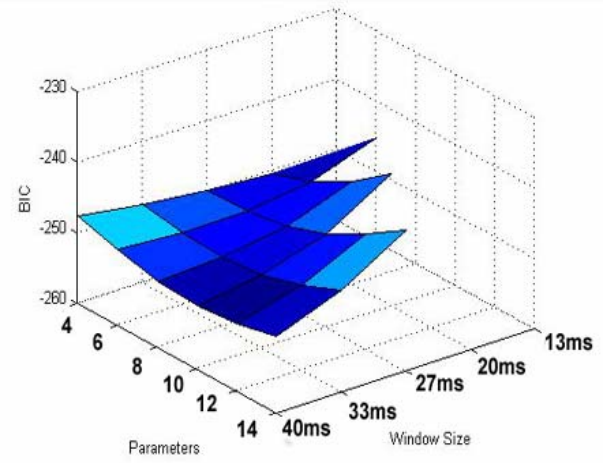

Fig 3. BIC values across model orders and window sizes for the gamma band frequency. Note that BIC is minimum at a model order of approximately 10 and a window size between 40ms and 33ms.

Each figure is a separate frame of a movie that can be viewed to consider the sequence of dynamic connectivity. A smoothing parameter is used to allow an appropriate transition of the connections from one movie frame to the next. Examining these movies showed several patterns of connectivity (Figs 4-8).

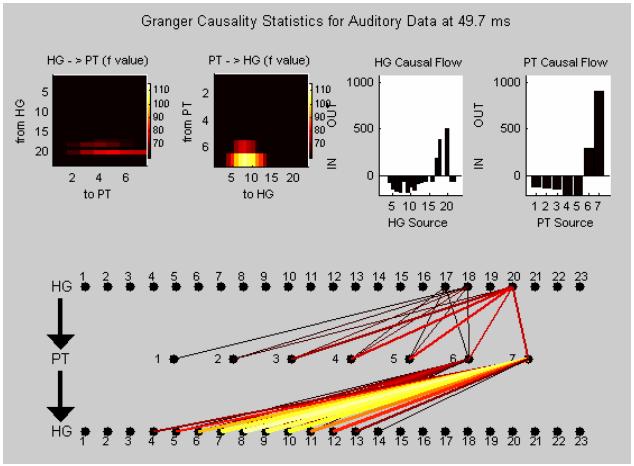

Fig 4. Connectivity between HG and PT within the beta frequency range early in perception of the /ba/ auditory syllable. Note the strong top-down connectivity from PT to HG with lesser bottom-up connectivity from HG to PT [F-value threshold = 60.0, Smoothing = 8].

The first observations found was that the pattern of dynamic connectivity was dependent on the frequency range. Figs 4 and 5 display two movie frames depicting dynamic connectivity for the beta frequency range. During the time course (movie) of the beta frequency range, the connectivity between PT and HG changed little with a large amount of connectivity from PT to HG throughout and only a transient influence of HG on PT in the initial stages of the time course.

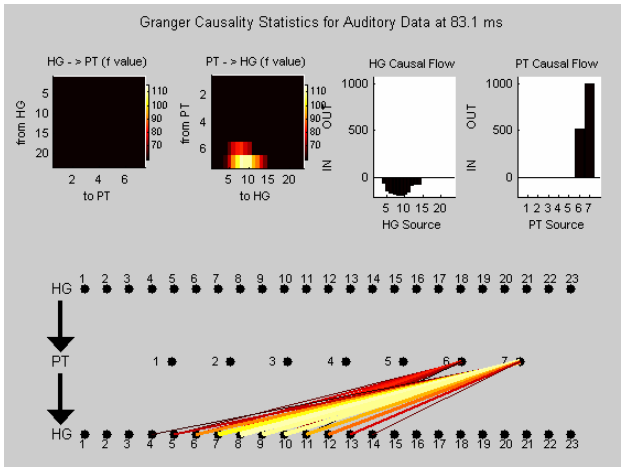

Fig 5. Connectivity between HG and PT within the beta frequency range late in perception of the /ba/ auditory syllable. Compared to Fig 4, the strong top-down connectivity from PT to HG remains but the lesser bottom-up connectivity from HG to PT has dissipated. [F-value threshold = 60.0, Smoothing = 8].

The pattern for the gamma frequency band was much different (Figs 6-8). Wide spread connections were demonstrated in both directions during the initial time course (Fig 6).

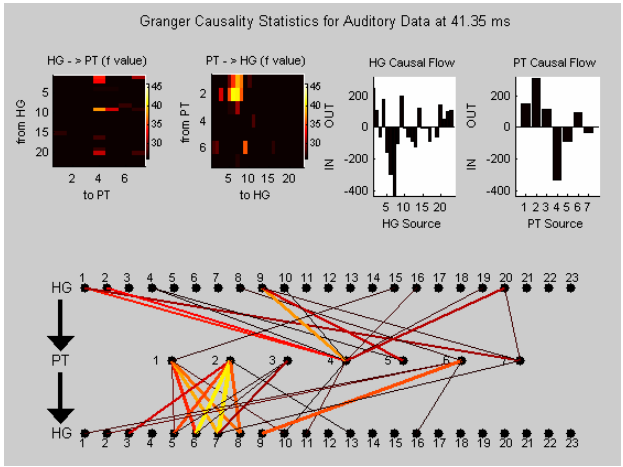

Fig 6. Connectivity between HG and PT within the gamma frequency range very early in the perception of the /ba/ auditory syllable. Note the numerous top-down and bottom-up connections from many sources to many other sources. [F-value threshold = 26.0, Smoothing = 5].

Later in the time course we see that these connections simplify and stabilize with several episodes during which specific PT sources influence specific HG sources and visa-versa.

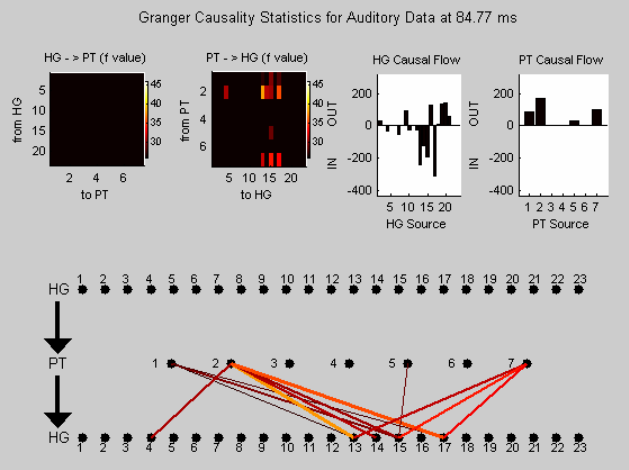

Fig 7. Connectivity between HG and PT within the gamma frequency range during perception of the /ba/ auditory syllable. During an approximate 20ms interval there appeared to be a strong convergence of top-down influence from specific PT sources (1,2,5,7) on to specific HG sources (13,14,15,17) [F-value threshold = 26.0, Smoothing = 5].

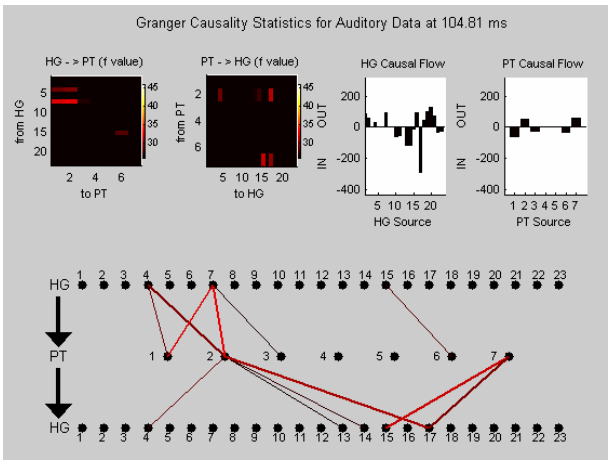

Fig 8. Connectivity between HG and PT within the gamma frequency range during perception of the /ba/ auditory syllable. Approximately 20ms after the strong top-down influence seen in Fig 7, strong bottom-up connections develop. Here we see that specific HG sources (4,7) converge on specific PT sources (1,2) [F-value threshold = 26.0, Smoothing = 5].

Fig 7 demonstrates organization of top-down connections whereby specific sources in PT influence specific sources in HG. Fig 8 demonstrates that this is followed by the development of strong bottom-up connections whereby specific HG sources influence specific sources in PT. These volleys of recurrent and reciprocal influence between these two areas suggest that that feedback and feedforward connections work together during syllable perception. This is consistent with predictions of neural models of speech perception [8].

4 Conclusion

This technique, which we will call Dynamic Autoregressive Neuromagnetic Causality Imaging (DANCI), has the capability to allow the visualization of dynamic functional connectivity and causality between important brain regions during whole-head MEG recording. Neural network structure and dynamics can be appreciated with this technique.

Development of this technique will require further investigation and validation:

- The effect of model order and window size on connectivity should be studied to determine whether the AIC and BIC statistics are sufficient for choosing these model parameters. For example these parameters may also be dynamic, require the structure of the model itself to change dynamically with time.
- The optimal manner in which to visualize connectivity needs to be studied. For example, although the prominent connections are visualized, the flow statistics do not always coincide with the visualized connections. This may suggest that many connections with values under the significance threshold are contributing to connectivity within certain sources.
- Not all source models by the ARMs demonstrate significant connections. Thus, the calculation for the solution of all of the connections performs unnecessary computations. Identifying and eliminating non-connected sources that are unlikely to demonstrate significant connections before the ARMs are constructed will allow more efficient computation of GC values.
- The sources produced by the dSPM technique are placed equally throughout on the cortex without regard for the location of the cortical activity. Thus, several sources may represent the same cortical activity while other sources may represent combinations of activity. Optimizing the placement of cortical sources will optimize the DANCI calculations.
- Functional mapping of the GC values on the inflated cortex will provide a better understanding of the significant of the connectivity patterns observed using the current DANCI technique.

Overall, the DANCI technique appears to be promising. Most importantly, this technique may be useful for validating various hypothesized neural network models and allow us to understand the small, medium and large-scale dynamics of brain function.

References:

[1] Ramnani N, Behrens TE, Penny W, Matthews, PM. New approaches for exploring anatomical and functional connectivity in the human brain, *Bio. Psychiatry,* Vol. 56, No. 9, 2004, pp. 613–619.

[2] Sherbondy A, Akers D, Mackenzie R, Dougherty R, Wandell B. Exploring connectivity of the brain's white matter with dynamic queries, *IEEE Trans Vis Comput Graph*, Vol. 11, No 4, 2005, pp. 419-430.

[3] Shaywitz SE, Shaywitz BA, Fulbright RK, Skudlarski P, Mencl WE, Constable RT, Pugh KR, Holahan JM, Marchione KE, Fletcher JM, Lyon GR, Gore JC. Neural systems for compensation and persistence: young adult outcome of childhood reading disability, *Biol Psychiatry,* Vol.54, No. 1, 2003, pp. 25-33.

[4] Astolfi L, Cincotti F, Mattia D, de Vico Fallani F, Lai M, Baccala L, Salinari S, Ursino M, Zavaglia M, Babiloni F, Comparison of different multivariate methods for the estimation of cortical connectivity: simulations and applications to EEG data. *Conf Proc IEEE Eng Med Biol Soc*, Vol. 5, 2005, pp. 4484-4487.

[5] Ding M, Bressler SL, Yang W, Liang H, Short-window spectral analysis of cortical event-related potentials by adaptive multivariate autoregressive modeling: data preprocessing, model validation, and variability assessment. *Biol Cybern*, Vol. 83, No. 1, 2000, pp. 35-45.

[6] Seth AK, Causal connectivity of evolved neural networks during behavior, *Network*, Vol. 16, No. 1, 2005, pp. 35-54.

[7] Lin FH, Belliveau JW, Dale AM, Hamalainen MS, Distributed current estimates using cortical orientation constraints, *Hum Brain Mapp*, Vol. 27, No. 1, 2006, pp. 1-13.

[8] Grossberg S, Govindarajan KK, Wyse LL, Cohen MA, ARTSTREAM: a neural network model of auditory scene analysis and source segregation, *Neural Netw*, Vol. 17, No. 4, 2004, pp. 511-536.